

JGR Solid Earth



RESEARCH ARTICLE

10.1029/2022JB025735

Key Points:

- We develop a rapid first-order method to correct the infrasound propagation backazimuth deviation for source location procedures
- We evaluate the method using long-range International Monitoring System data (~700-5,000 km) from the eruptions of Puyehue-Cordón Caulle (2011) and Calbuco (2015)
- We achieve a considerable source mislocation reduction for both eruptions (~75%–85%)

Supporting Information:

Supporting Information may be found in the online version of this article.

Correspondence to:

R. De Negri, rsd00@ucsb.edu

Citation:

De Negri, R., & Matoza, R. S. (2023). Rapid location of remote volcanic infrasound using 3D ray tracing and empirical climatologies: Application to the 2011 Cordón Caulle and 2015 Calbuco eruptions, Chile. *Journal of Geophysical Research: Solid Earth*, 128, e2022/B025735. https://doi.org/10.1029/2022JB025735

Received 5 OCT 2022 Accepted 18 FEB 2023

Author Contributions:

Conceptualization: Rodrigo De Negri, Robin S. Matoza

Data curation: Rodrigo De Negri, Robin S. Matoza

Formal analysis: Rodrigo De Negri, Robin S. Matoza

Funding acquisition: Robin S. Matoza **Investigation:** Rodrigo De Negri, Robin S. Matoza

Methodology: Rodrigo De Negri, Robin S. Matoza

© 2023. The Authors.
This is an open access article under the terms of the Creative Commons
Attribution-NonCommercial-NoDerivs
License, which permits use and distribution in any medium, provided the original work is properly cited, the use is non-commercial and no modifications or adaptations are made.

Rapid Location of Remote Volcanic Infrasound Using 3D Ray Tracing and Empirical Climatologies: Application to the 2011 Cordón Caulle and 2015 Calbuco Eruptions, Chile

Rodrigo De Negri¹ and Robin S. Matoza¹

¹Department of Earth Science and Earth Research Institute, University of California, Santa Barbara, Santa Barbara, CA, USA

Abstract Infrasound (<20 Hz) can propagate thousands of kilometers through the atmosphere, enabling global source location using networks of arrays such as the International Monitoring System infrasound network. However, atmospheric spatiotemporal variability poses a major challenge to locating infrasound sources. Strong horizontal cross-winds deviate the observed infrasound arrival azimuths, producing source mislocations that can be on the order of hundreds of kilometers. We introduce a method that combines empirical climatologies (HWM14/NRLMSIS2.0) and 3D ray tracing (infraGA) to obtain first-order, robust, and rapid estimates of the backazimuth deviations for source location procedures. For each trial source node and receiver path, day of the year and time, we perform an automatic iterative search for infrasound ground intercepts around the target station and obtain the corresponding backazimuth deviation. We test the method using IMS infrasound data from stations up to ~5,000 km range for two similar explosive eruption case studies: 2011 Puyehue-Cordón Caulle and 2015 Calbuco. We obtain a source mislocation reduction up to ~84% (242–38.7 km) and ~75% (366–93.1 km) for Puyehue-Cordón Caulle and Calbuco eruptions, respectively. To evaluate the approach, we repeat the procedure using more realistic hybrid atmospheric descriptions; we obtain comparable results (up to ~75% mislocation reduction for both eruptions). Potential applications of the approach include long-range volcano monitoring in near-real time by using pre-computed look-up tables or large-scale, multi-year reanalyses of infrasound waveform archives.

Plain Language Summary Acoustic waves below the human audible frequency range (20 Hz) are called infrasound. Favorable stratospheric wind conditions allow explosive volcanic infrasound to propagate hundreds to thousands of kilometers. The International Monitoring System (IMS) infrasound network can be used to detect and locate volcanic infrasound sources globally, but the atmospheric winds introduce deviations in the location of the sources that can be up to hundreds of kilometers from true. We introduce a method to generate rapid first-order azimuth corrections to tackle this issue, and test it with data from 2011 Puyehue-Cordón Caulle and 2015 Calbuco eruptions, Chile. We use infrasound detections from the nearest eight IMS stations to both volcanoes (~1,500 to ~5,000 km), obtaining significant improvements of the source locations (up to ~84% mislocation reduction). Upon further testing, this method could be used to improve long-range volcano monitoring in near-real time or large-scale, multi-year reanalyses of infrasound waveform archives.

1. Introduction

Detecting, quantifying, and cataloging the global occurrence of explosive volcanism helps toward several goals in Earth sciences and has direct applications in volcanic hazard mitigation (Matoza et al., 2019, and references therein). Previous work has demonstrated that infrasound arrays can be used to detect, locate, and provide detailed chronologies of remote explosive volcanism, with the potential to provide source parameters for ash transport and dispersal models (e.g., Caudron et al., 2015; Dabrowa et al., 2011; Fee et al., 2010; Garcés et al., 2008; Green et al., 2013; Marchetti et al., 2019; Matoza et al., 2007; Matoza et al., 2018; Matoza, Le Pichon et al., 2011; Matoza, Vergoz, et al., 2011; Perttu et al., 2020; Ripepe et al., 2018; Taisne et al., 2019). Regional volcano-acoustic monitoring and early warning systems are being investigated and implemented (De Angelis et al., 2012; Fee et al., 2010; Garcés et al., 2008; Kamo et al., 1994; Matoza et al., 2007; Ripepe et al., 2018; Taisne et al., 2019). Recent work has explored the potential of the International Monitoring System (IMS) infrasound network to provide a quantitative catalog of global explosive volcanic activity (Matoza et al., 2017) and automated eruption notifications to Volcanic Ash Advisory Centers (VAACs) (Mialle et al., 2015).

DE NEGRI AND MATOZA 1 of 18



Journal of Geophysical Research: Solid Earth

10.1029/2022JB025735

Resources: Robin S. Matoza **Software:** Rodrigo De Negri, Robin S.

Matoza

Supervision: Robin S. Matoza **Validation:** Rodrigo De Negri, Robin S.

Matoza

Visualization: Rodrigo De Negri, Robin

S. Matoza

Writing - original draft: Rodrigo De

Negri, Robin S. Matoza

Writing – review & editing: Rodrigo De

Negri, Robin S. Matoza

Required elements of a processing workflow to achieve these goals include infrasound signal detection, discrimination, association, and location (e.g., Arrowsmith et al., 2008; Arrowsmith et al., 2015; Arrowsmith & Whitaker, 2008; Brachet et al., 2010; Brown et al., 2002; Evers & Haak, 2005; Le Pichon et al., 2008; Modrak et al., 2010; Park et al., 2014; Sanderson et al., 2020). Challenges to each processing stage result from strong signal variability associated with long-range acoustic propagation through the temporally and spatially varying atmosphere (e.g., J. Assink et al., 2019; Drob, Garcés, et al., 2010; Le Pichon et al., 2009; Green & Bowers, 2010; Nippress et al., 2014; Waxler et al., 2017), and from widely varying incoherent wind noise (e.g., Walker & Hedlin, 2010) and coherent ambient infrasound (clutter) interfering sources (Matoza et al., 2013, 2019).

Here, our emphasis is on developing a method that could be applied rapidly to produce near-real-time analysis products to aid volcano monitoring, or that could be applied automatically and systematically to large data archives. Thus, we seek to provide rapid, first-order location solution estimates using automated procedures that do not require downloading and manipulating large realistic atmospheric specification products, emphasizing rapid and efficient computation speed over atmospheric and infrasound propagation realism (e.g., Schwaiger et al., 2019; Smets et al., 2015, 2016).

Stratospheric and lower mesospheric zonal winds have a strong influence on the observed wave parameters of infrasound detections (e.g., Drob, Meier, et al., 2010; Evers & Haak, 2005; Garcés, 2004; Le Pichon, Blanc, & Drob, 2005; Le Pichon, Blanc, Drob, et al., 2005; Le Pichon et al., 2006). At mid-to-high latitudes especially, the cross-winds at stratospheric heights become a primary factor controlling global infrasound source mislocation (e.g., Evers & Haak, 2005; Matoza, Le Pichon et al., 2011; Mialle et al., 2019), which has been up to hundreds of kilometers from true for IMS case studies (e.g., Evers & Haak, 2005; Matoza et al., 2017, 2019). A common approach for assessing the expected source mislocation is to forward-model the atmospheric effects on the infrasound detections (e.g., J. D. Assink et al., 2014; Arrowsmith et al., 2007; Le Pichon et al., 2009; Green et al., 2011; Marcillo et al., 2014; Matoza et al., 2018).

Atmospheric infrasound propagation modeling requires specifications of temperature, wind velocity, density, and molecular composition from the ground surface up to ~140 km altitude. To model infrasound propagation, these specifications are typically obtained in three main ways: (a) using data assimilation analyses such as the European Center for Medium-Range Weather Forecasting (ECMWF), which gathers ground-based and meteorological data as constraints to physically model the atmosphere from the ground to ~80 km in altitude every 6-hr; (b) empirical climatologies, which use multidecadal historical archives of the atmospheric data to statistically represent the atmosphere from the ground to the exobase (~750 km) with 12-hr intervals (e.g., the Horizontal Wind Model (HWM) (Drob et al., 2015) and the NRLMSIS2.0 model (Emmert et al., 2020); or (c) hybrid models that seamlessly integrate both approaches (e.g., the Naval Research Laboratory Ground to space (G2S) [Drob et al., 2003], or AVO-G2S [Schwaiger et al., 2019]). The most recent trend in infrasound studies is toward increasing propagation realism and accuracy (more accurate characterization of atmospheric state and finer spatio-temporal scales), implementing either data assimilation analyses or hybrid models (e.g., Ceranna et al., 2009; Fee et al., 2020; Smets et al., 2015). However, this comes with the cost of a greatly increased computational burden that can quickly escalate for global models and/or multi-decadal studies. Empirical climatologies, on the other hand, are succinct self-contained programs that reduce computational needs to a minimum, but generally underrepresent smaller scale atmospheric variations (e.g., stratospheric zonal jets) (Drob et al., 2003). Here we explore the potential of using empirical climatologies for a first-order "good enough" estimate of stratospheric cross-wind corrections for rapid infrasound signal association and source location, with the goal of realtime application or retrospective systematic reanalyses of large multi-decadal data archives. Our approach builds on that of pre-computed look-up tables, generally based also on empirical climatologies (e.g., Drob, Garcés, et al., 2010; Morton & Arrowsmith, 2014).

Matoza et al. (2017) introduced a signal association and location method algorithm (IMS_vASC), which uses array processing results from the global IMS infrasound network to automatically detect and catalog global multi-year (2005–2010) explosive volcanic signals. In this paper, we aim to incorporate first-order rapid corrections of the cross-winds effects on this trial source location process. Thus, we explore the use of empirical climatologies combined with infraGA 3D ray tracing (Blom & Waxler, 2012) to estimate the backazimuth deviation produced by the cross-winds for a large grid of trial source locations on the Earth's surface. Since infrasound propagation strongly depends on ducting conditions, we also investigate the use of a simplified Gaussian wind jet parameterization (Jones (1986) HARPA user manual) to perturb the climatology profiles and force a stratospheric or thermospheric return within reasonable bounds for the wind strength.

DE NEGRI AND MATOZA 2 of 18

21699356, 2023, 3, Downloaded from https://agupubs.onlinelibrary.wiley.com/doi/10.1029/2022JB025735, Wiley Online Library on [14/03/2023]. See the Terms

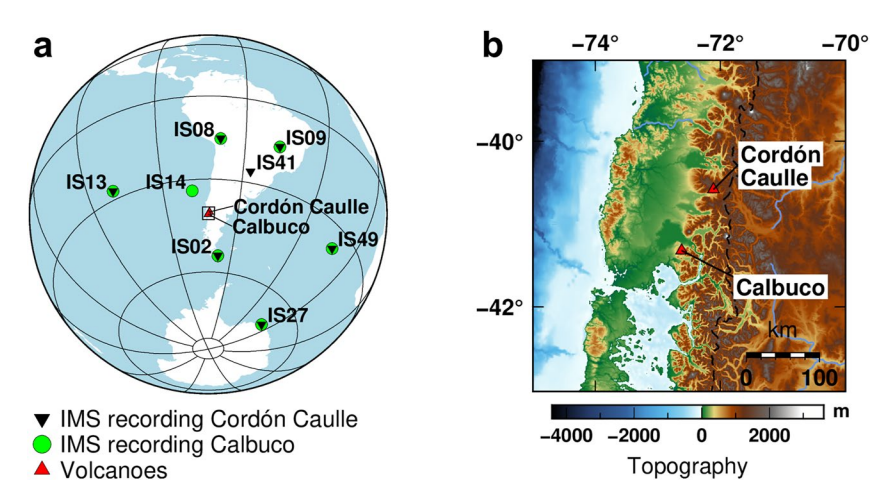


Figure 1. Location of International Monitoring System (IMS) stations and volcanoes. (a) Black inverted triangles: IMS stations that were recording during 2011 Puyehue-Cordón Caulle volcanic complex (Cordón Caulle) eruption. Green circles: IMS stations that were recording during the 2015 Calbuco eruption. Red triangles: PCCVC and Calbuco locations. Black rectangle indicates the zoomed area in (b). (b) Topographic map of the zoomed area of volcanoes (red triangles). Black-dashed line: border between Chile and Argentina.

In Section 2, we present two similar explosive eruption event case studies that we use to assess the method. In Section 3, we introduce the methodology to model the backazimuth deviations, as well as possible improvements to deal with the oversimplification of the lower atmospheric descriptions. In Section 4, we summarize our findings in reducing the source mislocation with IMS_vASC and compare the effects of choosing different atmospheric descriptions and modeling parameters. In Section 5, we discuss the feasibility of the method to obtain first-order approximations for global infrasound backazimuth deviations.

2. Data

2.1. Volcanic Setting

Puyehue-Cordón Caulle volcanic complex is a Pleistocene-Holocene active area composed of three volcanoes: Cordillera Nevada caldera (~1,000 m a.s.l), Cordón Caulle fissure system (~1,500 m a.s.l.), and Puyehue stratovolcano (~2,000 m a.s.l). It is located in the southern Andes volcanic zone, inside Puyehue National Park, Los Lagos Region, Chile (~40.5828°, ~72.1122°). Since the Late Pleistocene, Cordón Caulle has been the only active volcano, with at least three eruptions in the last century (1921, 1960 and 2011) (Elissondo et al., 2016). On 4 June at 18:45 UTC, 2011, after two months of increasing seismicity, the eruption started with an explosive event that generated a plume of ~9–12 km high (Collini et al., 2013; Elissondo et al., 2016). This paroxysmal plinian/subplinian phase lasted about 2 days, followed by a period of about 2 months with a fluctuating activity that resulted in sustained column heights between 4 and 12 km.

Calbuco volcano, Chile (-41.3300°, -72.6183°) is a ~2,000 m a.s.l. stratovolcano located at about 100 km SW from Cordón Caulle (Global Volcanism Program, 2013). On 22 April 2015, at 21:05 UTC, Calbuco started a subplinian/plinian explosive phase after a relatively short period of shallow seismic precursor activity, sending ash to an altitude of 15 km. The maximum intensity of the eruption was reached on April 23, with a phase of 6 hr in which column height reached 17 km (Castruccio et al., 2016; Matoza et al., 2018; Van Eaton et al., 2016). The intensity decreased rapidly after this phase, falling back into a pre-eruptive activity regime in about a month.

Cordón Caulle and Calbuco eruptions occurred at similar altitudes (~2,000 and ~1,500 m, respectively) and locations, under strong zonal mid-latitude eastward winds (see Figure 1; see also Figures S6 and S7 in Supporting Information S1). Both eruptions were cataloged as VEI 4 (volcanic explosivity index, [Newhall & Self, 1982]), with sustained plume heights of more than 10 km that lasted several days (Castruccio et al., 2016; Collini et al., 2013; Elissondo et al., 2016; Van Eaton et al., 2016), and occurred during atmospheric stratospheric winds prevailing toward the East.

DE NEGRI AND MATOZA 3 of 18

21699356, 2023, 3, Downloaded from https://agupubs.onlinelibrary.wiley.com/doi/10.1029/20221B025735, Wiley Online Library on [1 403/2023]. See the Terms and Conditions (https://onlinelibrary.wiley.com/terms-and-conditions) on Wiley Online Library for rules of use; OA articles are governed by the applicable Creaver Commons Licensia

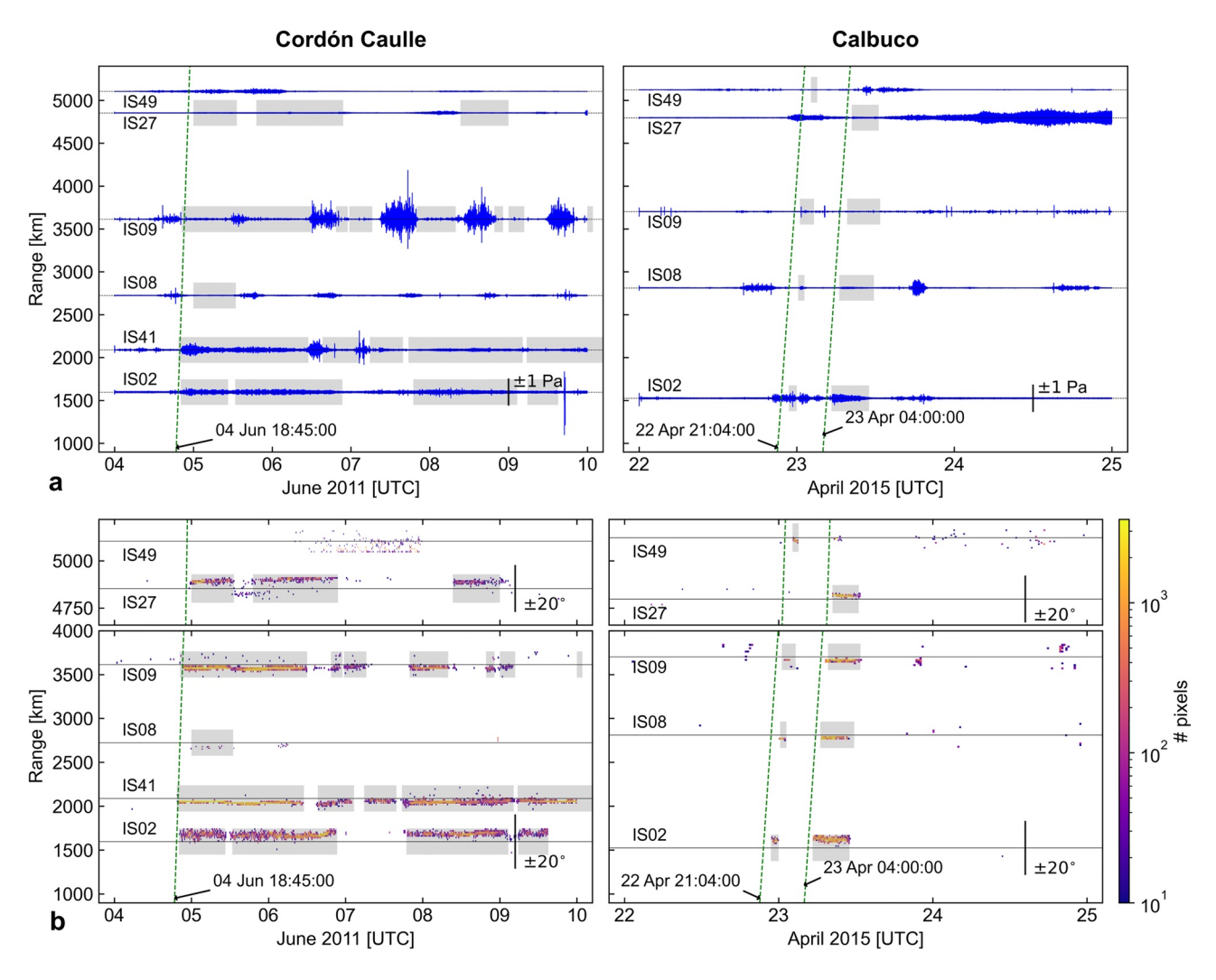


Figure 2. (a) Beamformed waveforms (0.5 < f < 5 Hz) for each station array, except upwind and non-recording stations (IS13, IS14, and IS41 for Calbuco only). In a gray background, we depict the associated detections attributable to the source in (b). In green slanted dashed lines, we show the estimated arrival time (c = 300 m/s) of the acoustic wave with origin time on each eruption's onset. (b) Progressive Multichannel Cross-Correlation (PMCC) detections from all available stations for Cordón Caulle (left) and Calbuco (right) volcanoes. For each station, we display a 2-D histogram that shows the number of pixels of parsed (0.5 < f < 5 Hz) PMCC detections in time (x-axis) by azimuth relative to the geographical station-to-source value (y-axis). Only values in the range $\pm 20^{\circ}$ for each station have been considered.

2.2. IMS Data

The IMS network is the main monitoring infrastructure of the Comprehensive Nuclear-Test-Ban Treaty Organization, integrating seismic, hydroacoustic, infrasonic, and radio nucleoid detection technologies. The IMS infrasound network currently has 53 (of 60 planned) stations detecting coherent acoustic waves that could be generated by explosions down to 1 kt of TNT anywhere on Earth (Christie & Campus, 2010). Each IMS station is composed of at least four microphone sensors with a flat response from 0.02 to 4 Hz within 3 dB. At the International Data Center of the CTBTO (Vienna, Austria) the raw waveforms from all IMS stations are processed with the Progressive Multichannel Cross-Correlation method algorithm (PMCC) (Cansi, 1995; Cansi & Klinger, 1997) in real-time, generating detection lists.

For this study, we considered the nearest eight IMS infrasound stations to both volcanoes (see Figure 1), which range from ~1,600 (IS02, Argentina) to ~5,100 km (IS49, United Kingdom). We downloaded the available IMS waveforms in a time window of 20 days, centered at each eruption time. We use PMCC to extract coherent detections for further analysis (see Figure 2 for a glance at the most interesting sequences). We implemented PMCC with 15 log-spaced frequency bands between 0.01 and 5 Hz, following Matoza et al. (2013).

DE NEGRI AND MATOZA 4 of 18

21699356, 2023, 3, Downloaded from https://agupubs.onlinelibrary.wiley.com/doi/10.1029/20221B025735, Wiley Online Library on [14/03/2023]. See the Terms and Conditions (https://or

We note that during the Cordón Caulle eruption (2011), the station IS14 was not operational after the destructive effects of the tsunami generated by the Chilean M8.8 Maule earthquake on 27 February 2010. Similarly, during Calbuco eruption (2015), station IS41 could not provide detections due to a reduced number of detecting channels (see Figure 1). We discuss the effects of the consequent station distribution difference in Section 5.

3. Methods

IMS_vASC is a brute-force, grid-search, cross-bearings method (Matoza et al., 2017) to localize sustained explosive volcanic infrasound signals with the IMS infrasound network of arrays. It enhances sources that have a sustained but limited time span (i.e., volcanic eruptions) by cleaning unwanted background detections (clutter) from the data. It localizes the source by performing cross-bearings for the nearest detecting stations with the backazimuth information of the cleaned detections. Although this approach takes advantage of the IMS infrasound network capabilities, atmospheric winds in the propagating path of the signals can considerably alter their apparent backazimuths and detectability (see Figure 3), causing source mislocations up to hundreds of kilometers (e.g., Drob, Meier, et al., 2010; Evers & Haak, 2005; Garcés, 2004; Le Pichon, Blanc, & Drob, 2005; Le Pichon, Blanc, Drob, et al., 2005; Le Pichon et al., 2006). IMS_vASC allows the use of backazimuth correction values in the source location process, but lacks a robust process to implement it. Thus, we aim to estimate the expected backazimuth deviations by modeling infrasound propagation under reasonable atmospheric conditions, providing IMS_vASC with a set of corrections to reduce the source mislocation. Once some basic parameters are defined (e.g., source and station locations, time, etc.), our approach automatically performs an iterative calculation of expected backazimuths (if any) by modeling infrasound propagation with 3D ray tracing (infraGA) (Blom & Waxler, 2012), and an empirical set of atmospheric descriptions obtained from a combination of the Horizontal Wind Model (HWM14) (Drob et al., 2015) and the Mass Spectrometer Incoherent Radar Model (NRLMSIS2.0) (Emmert et al., 2020).

3.1. Modeling the Atmosphere

3.1.1. Raw Climatologies

The "raw" climatological descriptions refer to the default atmospheric model obtained by combining HWM14 and NMRLSIS2.0. For each source-station direction and time, we obtain the horizontal winds (i.e., zonal and meridional), temperature, density, and pressure values every 50 km. For heights from 0 to 170 km in steps of 0.5 km, we average each parameter along the source-station direction, thus obtaining one set of estimations per height. The resulting model will be a layered range-independent atmosphere representative of each ray propagation direction, which is saved in tables (1D profiles) that will be used by the ray tracing algorithm to model infrasound ray propagation on a 3D spherical layered atmosphere. For the next atmospheric model types, the discretization follows the same procedure.

The strong assumption of a range-independent atmosphere is a reasonable first-order approximation that allows a reduced computational cost for 3D ray tracing propagation (see the infraGA/geoAC manual). As we use real observations to evaluate the validity of our approach, the comparison with more realistic but computationally demanding models (e.g., range-dependent ray propagation) should be considered in future developments (e.g., see Figure S19 in Supporting Information S1).

For this study, the eruption times are 2011-06-04 at 19:00 UTC for Cordón Caulle, and 2015-04-22 at 21:00 UTC for Calbuco.

In addition to the raw empirical climatologies used by default, we explore perturbing the wind values obtained with HWM14 to enhance along-path stratospheric winds in a simplified manner.

3.1.2. Perturbed Climatologies

Numerous case studies (e.g., Arrowsmith et al., 2007; J. D. Assink et al., 2014; Ceranna et al., 2009; Evers & Haak, 2007; Green et al., 2011; Lalande & Waxler, 2016; Le Pichon et al., 2015; Smets et al., 2016) have shown that long-range infrasound detection is often dependent on marginal ducts. Smoothed atmospheric profiles available in both weather reanalysis products and climatologies fail to capture small-scale fluctuations on which infrasound propagation depends, thus controlling detection versus non detection for a source-receiver pair

DE NEGRI AND MATOZA 5 of 18

21699356, 2023, 3, Downloaded from https://agupubs.onlinelibrary.wiley.com/doi/10.1029/20221B025735, Wiley Online Library on [14/03/2023]. See the Terms and Conditions (https://onlinelibrary.wiley.com/terms

and-conditions) on Wiley Online Library for rules of use; OA articles are governed by the applicable Creat-

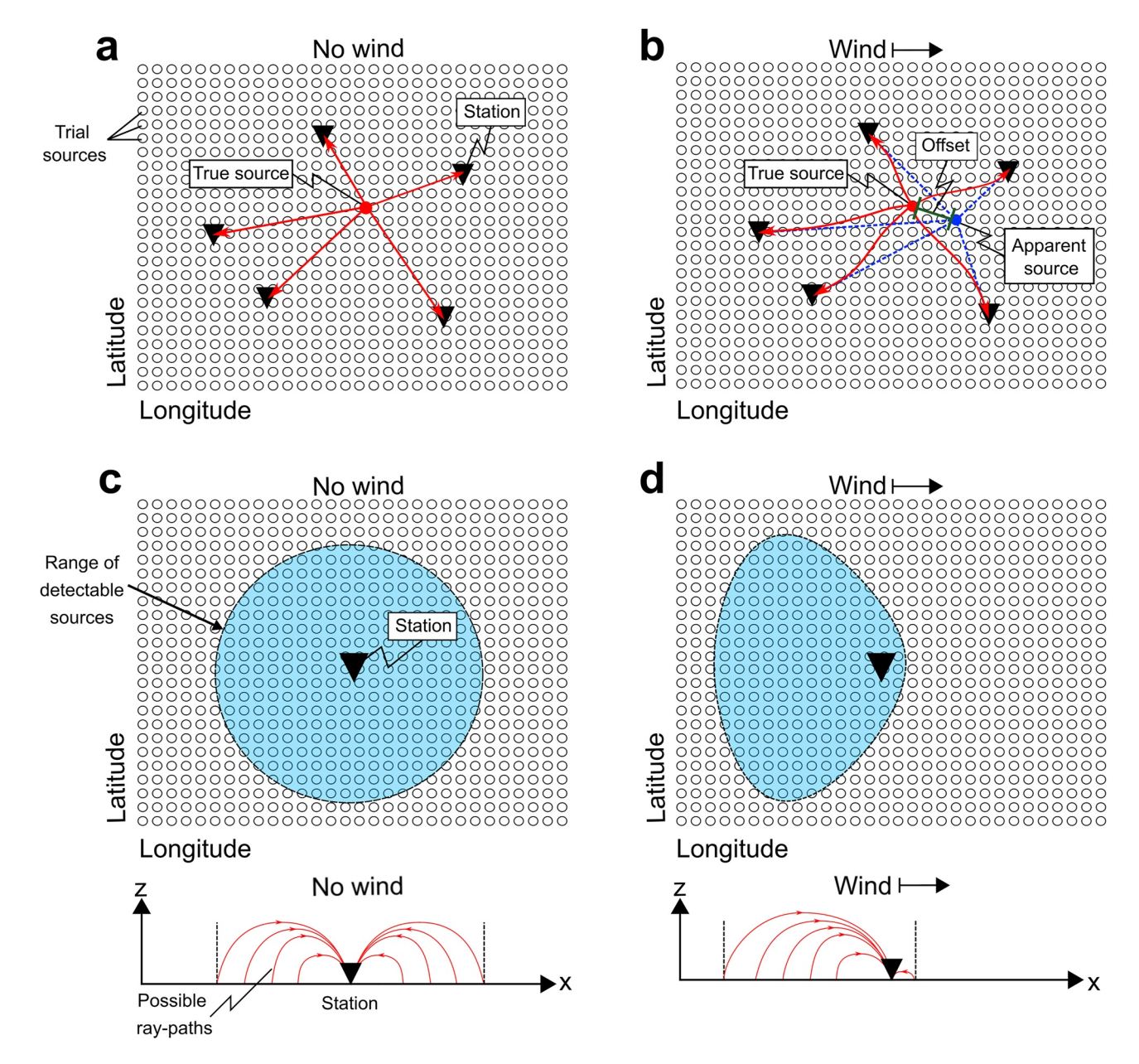


Figure 3. Effect of stratospheric winds on the source offset (top) and the source detectability (bottom). The stations are depicted as black inverted triangles, while the possible trial sources as a grid of white circles surrounding them. (a) A source (red circle) produces signals that travel undisturbed to each station (no wind present). (b) The moving medium (i.e., winds), bends the ray paths (red). Under winds blowing from west to east, the source seems to be shifted eastwards when performing cross-bearing locations with the apparent backazimuths (blue dashed line), producing an offset. (c) Without winds, the detectable sources should be inside the light-blue circle around the station (black triangle). (d) With wind blowing from west to east as shown in this figure, the detectable range is now enhanced in the downwind direction from the trial sources or similarly the upwind direction from the station (i.e., here more trial sources to the West of the station are possible candidates for signals detected by the station). Conversely, the detectable range is reduced in the downwind direction (East) from the station (corresponding to the upwind direction from these trial sources East of the station toward this station). Cartoons of example ray paths in 2D show how the wind affects detectability at the bottom of (c and d).

(e.g., Matoza, Le Pichon et al., 2011). A fundamental limit of the climatologies used in this study is that they tend to underestimate the atmospheric propagation ducts. In prior studies, this issue has been tackled by using gravity-wave perturbations of the profiles to obtain more realistic infrasound arrivals (ground intercepts) (e.g., Gibson et al., 2009; Green et al., 2011; Kulichkov et al., 2010; Norris et al., 2010; Smets et al., 2016). However, this type of approach tends to be computationally expensive, departing from our rapid first-order main goal. Instead, we investigate the use of a simplified parametric Gaussian wind jet (Jones, 1986) perturbation to enhance the stratospheric winds that could cause ducting (see Figure 4). The perturbation is centered at 40 km of altitude,

DE NEGRI AND MATOZA 6 of 18

21699356, 2023, 3, Dowlonded from https://agupubs.onlinelibrary.wiley.com/doi/10.1029/20221B02735, Wiley Online Library on [1.403/2023]. See the Terms and Conditions (https://onlinelibrary.wiley.com/terms-and-conditions) on Wiley Online Library for rules of use; OA articles are governed by the applicable Creative Commons Licensea

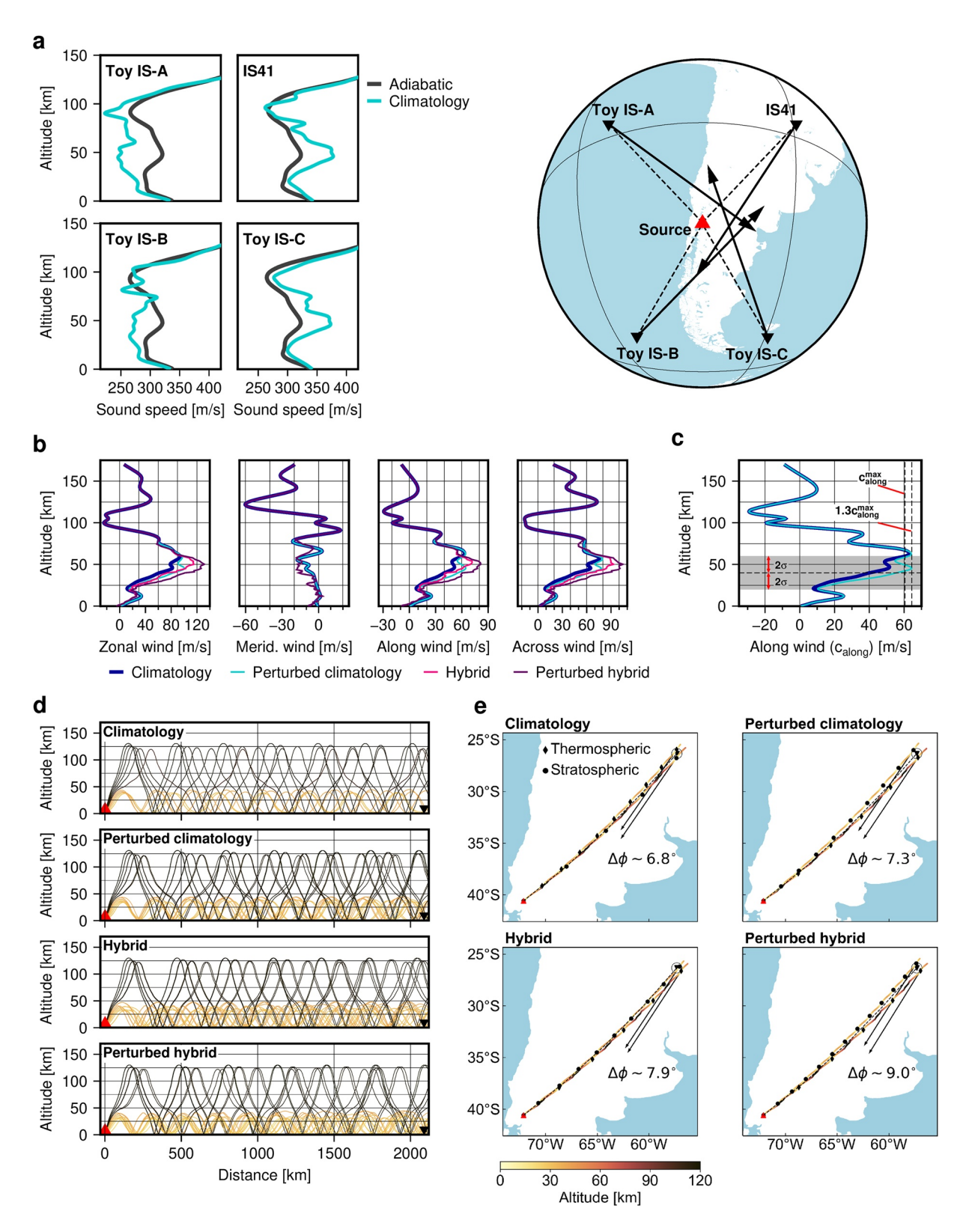


Figure 4.

DE NEGRI AND MATOZA 7 of 18

21699356, 2023, 3, Downloaded from https://agupubs.onlin

elibrary.wiley.com/doi/10.1029/2022JB025735, Wiley Online Library on [14/03/2023]. See the Terms and Conditions

conditions) on Wiley Online Library for rules of use; OA articles are governed by the applicable Creative Commons Licens

with a standard deviation of 10 km, and amplitude equivalent to 30% of the maximum effective speed (see Equation 1) in this altitude range (\sim 20–60 km; see Figures 4c and 4d). Additionally, the perturbation is applied only when positive along-path winds are present at these altitudes to avoid creating unrealistic zonal ducts.

$$c_{eff} = c_T + \hat{n} \cdot \vec{c}. \tag{1}$$

where $\vec{c} = (u, v)$ is the wind speed in height, with u and v the zonal and meridional winds, respectively; \hat{n} is the propagation direction from the source to the station; and c_T is the adiabatic sound speed in height.

We note that this simplified wind perturbation approach is justifiable given the method application in a grid-search source location procedure (Matoza et al., 2017). In this procedure, a trial source node is only illuminated if there are corresponding observed detections at multiple stations. Thus, the Gaussian wind jet is simply a tool to help assess if a given trial source node is feasible for a given set of infrasound observations given reasonable deviations of the atmospheric profiles.

We assess how the raw and perturbed climatologies results compare to more realistic atmospheric descriptions corresponding to a hybrid model based on the European Centre for Medium-Range Weather Forecasts (ECMWF) descriptions.

3.1.3. Hybrid Model

We build a hybrid set of descriptions by merging the ECMWF reanalysis v5 (ERA5) data for the model reference levels (137 levels from \sim 0 to \sim 80 km altitude) with empirical climatologies (>80 km altitude) in height (see Figure 4). We download ERA5 descriptions of horizontal winds and temperature for the area and time of interest, and complete the descriptions in height with the empirical climatologies using a simple linear interpolation of the averaged in values per height. This results in more realistic wind and temperature descriptions under \sim 80 km altitude for the infrasound raypaths (i.e., small tropospheric or stratospheric ducts), completed above \sim 80 km with the robust but coarser climatological descriptions (See Figures S2–S5 in Supporting Information S1).

3.1.4. Perturbed Hybrid Model

We also calculate a set of perturbed hybrid profiles following the same procedure as in Section 3.1.2. In this case, the resulting descriptions will not match the realistic model, but could account for other type of phenomena that are still not present in the ERA5 profiles (i.e., gravity waves types of perturbations).

Once the atmosphere model is defined, we continue with an iterative approach to determine the backazimuth deviation for each source-station pair.

3.2. Iterative Backazimuth Deviation Estimation

For a given trial source node and receiver (station) pair, we begin by using infraGA 3D ray tracing to launch two sets of rays, with azimuths ϕ_1 and ϕ_2 , that azimuthally enclose the station location (see Figure 5, left panel). The launch azimuths are modified iteratively to converge to a value where it is possible to obtain ground intercepts or to otherwise declare the case as "ill-conditioned" (no ground arrivals near the station). Both sets of rays, with corresponding backazimuths φ_1 and φ_2 , are launched with inclinations from 0.5° to 40.0° in steps of 0.5° . If the ground intercepts (depicted as white circles in 5, left panel) have a great-circle annular distance smaller than the threshold value, d_r (0.5° for this study), their backazimuths are averaged and used as a starting value to launch the next iteration. The next launching azimuths, ϕ'_1 and ϕ'_2 , are modified to reduce the great-circle radial distance from the average location of ground intercepts to the receiver, d_{ϕ} (Figure 5, right panel). This process continues until d_{ϕ} is reduced below a threshold value (0.05° for this study). Once the ground intercepts are near enough to

Figure 4. (a) Right: example case of cross-bearings for Cordón Caulle location (red triangle) during predominant Winter-like eastward zonal winds (the only real infrasound station is IS41). Here the source appears to be East of the true source location. In black arrows: modeled backazimuth from each station. In black-dashed lines: geographical azimuths from Cordón Caulle to each station (black inverted triangles). Left: reference average sound speed profiles in altitude calculated with empirical climatologies for each station. (b) Reference zonal, meridional, along-path, and across-path atmospheric winds in altitude for Cordón Caulle to IS41 direction, from empirical climatologies (blue line), perturbed climatologies (cyan line), hybrid (purple), and perturbed hybrid descriptions (pink). (c) Close-up comparison between empirical climatologies and perturbed climatologies, showing the heights where the empirical climatologies are perturbed to match $1.3 \times c_{along}^{max}$ (~20–60 km). (d) Comparison of ray tracing results for IS41 using the atmospheric descriptions in (b). The selected rays are colored by turning altitude (see color bar at bottom right). (e) Overhead maps with a stratospheric and a thermospheric ray from (d). The rays are colored by altitude. The backazimuth deviations of each ray at IS41 ($\Delta\phi$) are depicted by black arrows, while the average azimuth deviation is indicated numerically in the map as well. The black dots and diamonds represent the stratospheric and thermospheric ray ground intercepts, respectively.

DE NEGRI AND MATOZA 8 of 18

21699356, 2023, 3, Downloaded from https://agupubs.onlinelibrary.wiley.com/doi/10.1029/20221B025735, Wiley Online Library on [14/03/2023]. See the Terms and Conditions

Figure 5. Iterative backazimuth deviation estimation for an a priori known source location (red dot). (a) The source has a geographical azimuth (blue line), or "true azimuth," toward the receiver (blue square). First, we launch two sets of rays (purple curved lines) with azimuths, ϕ_1 and ϕ_2 , containing the true azimuth, ϕ_{true} . The curvature of the launched rays represents the effect of eastward winds (black arrow on each subplot), introducing an backazimuth deviation. If the ground intercepts (white circles) are inside an annular area of width $2d_r$ (green intervals), their average (purple dot) is used to obtain their respective backazimuths, φ_1 and φ_2 . (b) Next, we reduce the angular distance and recalculate the backazimuths as in (a). The new launch azimuths (ϕ_1' and ϕ_2') still contain the true azimuth (ϕ_{true}), and should be inside the annular area in (a). We repeat this process iteratively until the desired threshold, d_{ϕ} , is reached. The final backazimuths, φ_1' and φ_2' , are averaged to determine the backazimuth deviation, $\Delta \varphi$, for the source-receiver pair.

the receiver, their average properties are calculated and used to determine the modeled backazimuth, φ_{app} . If a maximum number of attempts is exceeded during the search process (40 in this study), the case is also declared to be "ill-conditioned", reflecting atmospheric conditions that in practice will impede infrasound detections at the station (e.g., strong stratospheric winds that oppose the propagation direction). Finally, the backazimuth deviation, $\Delta \varphi$, is calculated as the difference between the geographical backazimuth, φ_{true} , and the modeled backazimuth, φ_{mod} (i.e., $\Delta \varphi = \varphi_{true} - \varphi_{mod}$).

We note that infraGA includes an eigenray search method that could be used for determining ray parameters as we did in this study. However, at the propagation ranges we consider (\sim 700 to \sim 5,000 km), the infraGA search method will be unable to find arrivals at the target stations, which is essentially due to the increasing launch angle sensitivity with range. Different approaches could also be used to deal with this issue (e.g., Blom, 2020).

4. Results

4.1. Waveforms and PMCC Detections

We display the waveforms and PMCC detections from the IMS stations considered in this study in Figure 2 from 1 day before each eruption onset to 5 days after for Cordón Caulle and 2 days after for Calbuco. We note IS41, the station with the longest PMCC detection sequence during Cordón Caulle eruption (Figure 2b, left), was not recording during Calbuco eruption (Figure 2b, right). Additionally, the lack of IS13 and IS14 records from Figure 2 was a choice to emphasize the most relevant stations detections, despite their datasets being still considered in our analysis (see Figure S1 in Supporting Information S1). The prevalence of strong eastern stratospheric winds during both eruptions (see Figures S6 and S7 in Supporting Information S1) made these stations unable to detect long-range infrasound coming from the east (i.e., upwind sound propagation).

The expected arrival times of the observed explosive eruption phases (Castruccio et al., 2016; Collini et al., 2013; Elissondo et al., 2016; Van Eaton et al., 2016) for celerities of 300 m/s across the stations (green dashed lines) help visualize the difference between the background PMCC detections before and after volcanic activity. For both volcanoes, the eruptive onset can be observed in at least four stations. These are IS02, IS41, IS09, and IS49 for Cordón Caulle; and IS02, IS08, IS09, and IS49 (first explosion) or IS27 (second explosion). On the other hand, it is clear that much of the observable waveforms do not match the coherent volcanic detections (gray boxes in Figure 2a).

DE NEGRI AND MATOZA 9 of 18

21699356, 2023, 3, Downloaded from https://agupubs.onlinelibrary.wiley.com/doi/10.1029/2022JB025735, Wiley Online Library on [14/03/2023]. See the Terms and Conditions

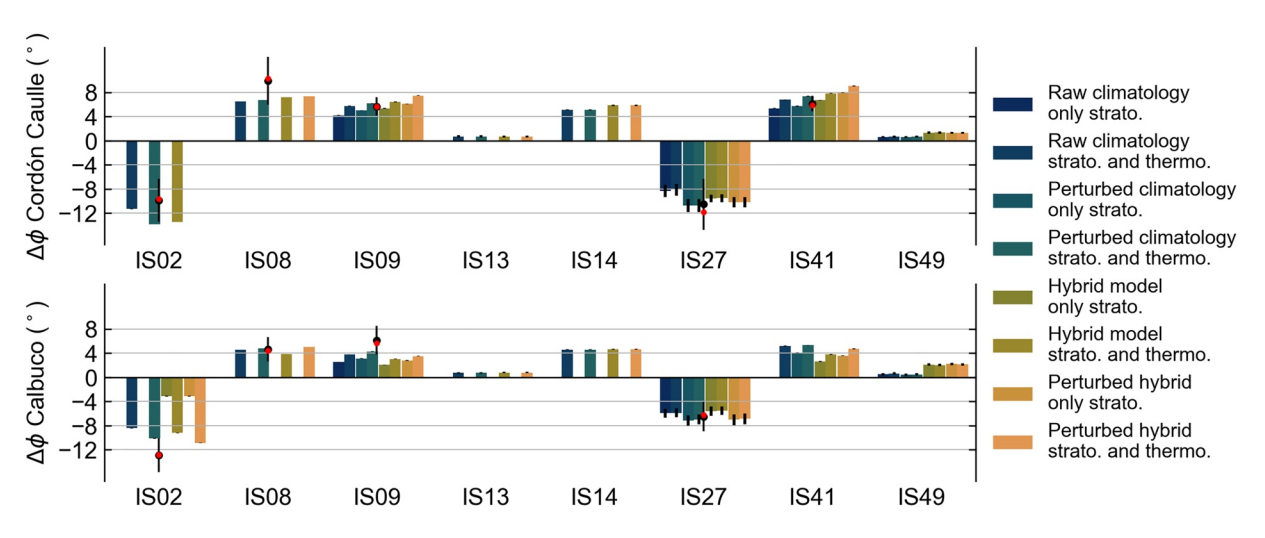


Figure 6. Comparison of backazimuth deviation results modeled for all considered stations for both eruptions. Each result is a combination of the model choices described in Section 3.1 using only arrivals that turned at stratospheric heights ("only strato."), or using arrivals that have both stratospheric and thermospheric turning heights ("strato. and thermo."). Each bar represents the backazimuth deviation value (see Section 3.2). Some of the stations do not have an associated backazimuth deviation, indicating the method does not converge. Each bar has a standard deviation size range indicated on a black vertical line. For the stations IS02, IS08, IS09, IS27 for both volcanoes, and IS41 for Cordón Caulle only, we show the real backazimuth deviation mean (black dot), median (red dot), and standard deviation (vertical black line) for the first two days since each eruption (Figure 2; Figures S11 and S12 in Supporting Information S1).

The general backazimuth deviation of the detections is similar for both eruptions, with stronger effects due to higher regional zonal winds for Cordón Caulle (June 2011) than Calbuco eruption (April 2015) (see Figures S2–S5 in Supporting Information S1 for effective sound speed profiles; also S6 and S7 for average zonal winds in area of study). The station coverage is affected by the zonal wind conditions, generating an azimuthal gap of detecting stations of (\sim 200°) on the western quadrant (IS02–IS08). The eastern quadrant stations (i.e., downwind signal propagation) have an azimuthal gap of \sim 107° instead (from IS09 to IS27), and carry the bulk of the detection information that will be used to find the most probable source location.

An evident difference between Cordón Caulle and Calbuco eruptions (Figure 2b) is that the PMCC infrasound detections last for at least 5 days for the former, while only some hours for the latter. The apparent source locations for both eruptions should be then determined by similar wind effects, but with a better station coverage (IS41) and a considerably higher number of detections for Cordón Caulle than Calbuco.

4.2. Predicted Backazimuth Deviations

For each atmosphere model defined in Section 3, we run a simulation to estimate the backazimuth deviation at each station for signals coming from both eruptions (Figure 6). Additionally, we classify our results by the turning height of the ground intercepts, labeling them as "only strato." when only using rays with stratospheric turning heights (<60 km), or "strato. and thermo." when also including ground intercepts with thermospheric turning heights (usually $\sim 120 \text{ km}$).

The modeled backazimuth deviations are positive (i.e., observed azimuth is smaller than the true azimuth) when the source-station direction has a north component, and negative (i.e., observed azimuth is bigger than true) on the opposite case, matching the observed deviations in Figure 2. The backazimuth deviation magnitudes range from $\sim 1^{\circ}$ (IS49) to $\sim 12^{\circ}$ (IS02), with higher values for Puyehue-Cordón Caulle (~ 2 to $\sim 12^{\circ}$) than for Calbuco (~ 1 to $\sim 10^{\circ}$), in concordance with stronger eastward zonal winds for June than April in the area of study (See Figures S6 and S7 in Supporting Information S1).

Near all "strato. and thermo." cases successfully provided deviation values, although IS13 and IS14 have associated deviations with extreme arrival transmission looses (see Figures S8 and S9 in Supporting Information S1) that render their predictions invalid for data correction purposes.

When "only stato." and "strato. and thermo." models give deviation estimates, we see the values are comparable, with generally smaller magnitudes for "only strato." results (e.g., IS90, IS27, IS41, or IS49). The exception to this rule is IS02 for Calbuco when using a hybrid model, where a strong tropospheric jet, invisible for the

DE NEGRI AND MATOZA 10 of 18

21699356, 2023, 3, Downloaded from https://agupubs.onlinelibrary.wiley.com/doi/10.1029/2022JB025735, Wiley Online Library on [14/03/2023]. See the Terms and Condition

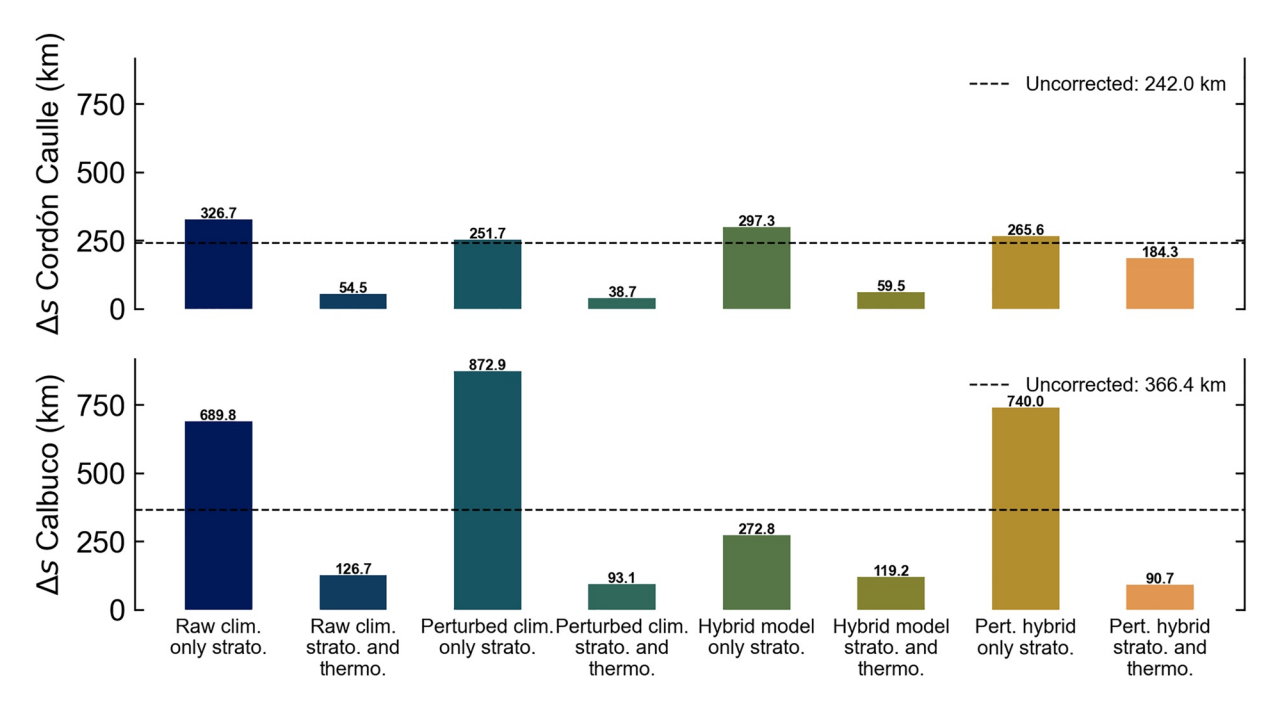


Figure 7. Summary of modeled source location offsets (km) using IMS_vASC for each combination of choices (see Figure 6). In a black-dashed line, we depict the offset when no corrections are used (i.e., "uncorrected").

climatologies, allows arrivals with a much smaller backazimuth deviation (see Figures S4 and S5 in Supporting Information S1).

For cases with enough detections and clear bell-like distributions (see Figures S11 and S12 in Supporting Information S1) we included estimations of the observed backazimuth deviation mean, median, and standard deviation in Figure 6 (IS02, IS08, IS09, and IS27 for both volcanoes, while IS41 only for Cordón Caulle). We see a general agreement of the observed mean and medians with the predicted values across all models, but especially the perturbed cases, as they produce higher backazimuth deviations. The climatologies compare well with the hybrid models, with backazimuth deviations that differ by $\sim 1-2^{\circ}$.

4.3. Source Locations

We first calculated the uncorrected (straight ray great-circle path assumption) source location with IMS_vASC, finding a mislocation of \sim 242 km for Puyehue-Cordón Caulle eruption that increased to \sim 366.4 km for Calbuco eruption (Figures 7 and 8). These values represent the baseline mislocation due to atmospheric conditions during each eruption.

After using the modeled backazimuth deviations (Figure 6) as correction values for IMS_vASC, we observe that regardless of the atmospheric model used, the mislocations reduce for all the "strato. and thermo." results (Figure 7), but almost always increase for the "only strato." results (only the Hybrid model reduces the mislocation).

For the Puyehue-Cordón-Caulle case, the \sim 242 km original offset reduces from \sim 24% (\sim 184.3 km, "Hybrid pert. strato. and thermo.") to \sim 84% (\sim 38.7 km, "Perturbed clim. strato. and thermo."). For Calbuco case (\sim 366.4 km), the reduction ranges from \sim 65% (\sim 126.7 km, "Raw clim. strato. and thermo.") to \sim 75% (90.7 km, "Pert. hybrid strato. and thermo.").

The association and location method, IMS_vASC, also finds the nearest Holocene potentially active volcano (Global Volcanism Program, 2013) after calculating the apparent location of the source. In Table 1, we summarize the apparent source and nearest active volcano mislocations to the actual targets. The climatological corrections have comparable mislocation reduction results with the hybrid corrections, with better results than the hybrid model when using perturbed climatologies with stratospheric and thermospheric arrivals.

DE NEGRI AND MATOZA 11 of 18

21699356, 2023, 3, Downloaded from https://agupubs.onlinelibrary.wiley.com/doi/10.1029/2022JB025735, Wiley Online Library on [1403/2023]. See the Terms and Conditions (https://onlinelibrary.wiley.com/rerms

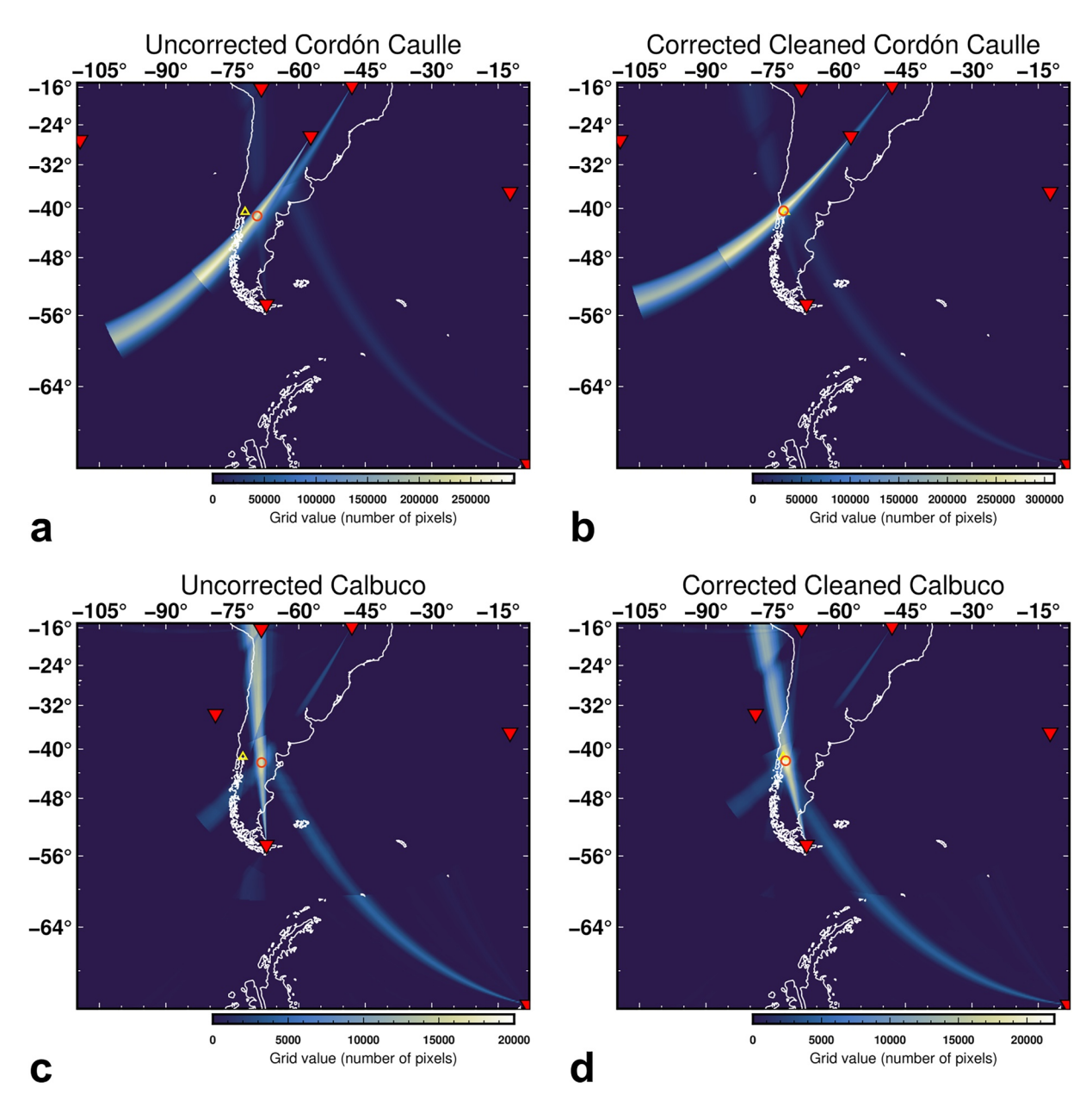


Figure 8. Left (a and c): uncorrected source locations with IMS_vASC for PCCVC and Calbuco volcanoes, with offsets of 242 and 366.4 km, respectively. Right (b and d): best source location results by absolute source location with IMS_vASC for Cordón Caulle and Calbuco volcanoes, with offsets of 38.7 and 90.7 km for the models "Perturbed clim. only strato." and "Perturbed hybrid strato. and thermo.", respectively (Figure 7). All source location plots correspond to the cleaned grid, G^c , results (Matoza et al., 2017).

5. Discussion

5.1. Crosswinds and Observed Detections

During the eruptions of Cordón-Caulle (June 2011) and Calbuco (April 2015) strong eastward seasonal winds occurred at stratospheric altitudes, producing similar effects on the infrasound propagation ray paths. West of both volcanoes, the upwind propagation direction of the signals left stations IS13 and IS14 unable to detect the eruptions. At the east, the downwind propagation direction favored long-range propagation that resulted in clear volcanic infrasound at most of the stations. With volcanic infrasound detection frequencies usually lower than 2 Hz, this is an expected effect of the yearly global stratospheric wind circulation patterns (Le Pichon et al., 2009). The observed backazimuth deviations (see Figure 2) follow the patterns of a source that seems to be "pushed" downwind (east, as illustrated in Figure 3b), producing azimuths that are smaller than true (i.e., positive deviation) for stations to the north

DE NEGRI AND MATOZA 12 of 18

21699356, 2023. 3, Downloaded from https://agupubs.onlinelibrary.wiley.com/doi/10.1099/202218025735, Wiley Online Library on [14/03/2023]. See the Terms and Conditions (https://onlinelibrary.wiley.com/doi/10.1099/202218025735, Wiley Online Library on [14/03/2023]. See the Terms and Conditions (https://onlinelibrary.wiley.com/doi/10.1099/202218025735, Wiley Online Library on [14/03/2023]. See the Terms and Conditions (https://onlinelibrary.wiley.com/doi/10.1099/202218025735, Wiley Online Library on [14/03/2023]. See the Terms and Conditions (https://onlinelibrary.wiley.com/doi/10.1099/202218025735, Wiley Online Library on [14/03/2023]. See the Terms and Conditions (https://onlinelibrary.wiley.com/doi/10.1099/202218025735, Wiley Online Library on [14/03/2023]. See the Terms and Conditions (https://onlinelibrary.wiley.com/doi/10.1099/202218025735, Wiley Online Library on [14/03/2023]. See the Terms and Conditions (https://onlinelibrary.wiley.com/doi/10.1099/202218025735, Wiley Online Library on [14/03/2023]. See the Terms and Conditions (https://onlinelibrary.wiley.com/doi/10.1099/202218025735, Wiley Online Library.wiley.com/doi/10.1099/202218025735, Wiley Online Library.wile

Journal of Geophysical Research: Solid Earth

Table 1

Volcano	Model	Abs. Δs (km)	Near. Δs (km)	Nearest volcano
	Uncorrected	242.0	226.3	Crater Basalt Field
	Raw clim., only strato.	326.7	228.8	Laguna Blanca
	Raw clim., strato. and thermo.	54.5	65.8	Osorno
Cordón	Pert. clim., only strato.	251.7	228.8	Laguna Blanca
Caulle	Pert. clim., strato. and thermo.	38.7	26.1	Carrán-Los Venados
	Hybrid model, only strato.	297.3	228.8	Laguna Blanca
	Hybrid model, strato. and thermo.	59.5	73.2	Mocho-Choshuenco
	Hybrid pert., only strato.	265.6	251.6	Tralihue
	Hybrid pert., strato. and thermo.	184.3	186.1	Sollipulli
	Uncorrected	366.4	215.7	Crater Basalt Field
	Raw clim., only strato.	689.8	537.8	Río Murta
	Raw clim., strato. and thermo.	126.7	52.5	Cuernos del Diablo
	Pert. clim., only strato.	872.9	983.7	Viedma
Calbuco	Pert. clim., strato. and thermo.	93.1	50.8	Yate
	Hybrid model, only strato.	272.8	215.7	Crater Basalt Volcanic Fie
	Hybrid model, strato. and thermo.	119.2	62.4	Hornopirén
	Hybrid pert., only strato.	740.0	537.8	Río Murta
	Hybrid pert., strato. and thermo.	90.7	62.4	Hornopirén

Note. "Abs. Δs (km)" refers to the distance between the obtained apparent source location to the true source location for each case. "Near. Δs (km)" refers to the distance between the nearest holocene-active volcano from the apparent location to the true location of the source.

> of both sources (e.g., IS08, IS09, and IS41), and larger than true (i.e., negative deviation) for stations to the south (e.g., ISO2 and IS27) of the sources (e.g., Evers & Haak, 2005; Matoza et al., 2018; Matoza, Le Pichon, et al., 2011).

5.2. Predicted Backazimuth Deviations

We see a general agreement between the predicted backazimuth deviations (Figure 6) and the observed backazimuth deviations (Figure 2b). The deviation magnitudes correlate with the crosswind strength along the propagation path of each profile. Stations south from both volcanoes show generally higher deviations than stations at the north, as the zonal winds were stronger at mid-to-high latitudes (see Figures S6 and S7 in Supporting Information S1). High deviations from arrivals that are only thermospheric are associated with near-north or near-south profiles (IS08 and IS02, respectively). High deviations where arrivals are mostly stratospheric are the product of strong crosswinds with an along-path component that increase the effective sound propagation of the signals (e.g., IS27, IS41, and IS09). Low deviations with stratospheric and thermospheric arrivals are present only for IS49, located almost downwind from both volcanos with a strong favorable stratospheric wind jet (see Figures S2-S5 in Supporting Information S1). Except for IS49, the farthest station considered (~5,000 km) with a subsequent high attenuation propagation, all detecting stations had observations with similar backazimuth deviations than our predictions (see Figure 6).

5.2.1. Thermospheric Arrivals

In cases when both "strato." and "strato. and thermo." models have associated backazimuth deviations, their values are similar (e.g., IS09, IS27, IS41, and IS49). The slightly higher average backazimuth deviation estimation for the "strato, and thermo," cases $(\sim 1^{\circ})$ is produced by the higher deviations thermospheric arrivals have in our models. The agreement between "strato." and "strato. and thermo." values, suggests that in cases where no stratospheric arrivals were found (e.g., stations IS02 and IS08 in Figure 6), thermospheric arrivals aid with modeling crosswind effects. This is also reinforced by the significant mislocation reduction obtained when applying corrections derived from "strato. and thermo." models (see Figure 7). Despite thermospheric

DE NEGRI AND MATOZA 13 of 18

21699356, 2023, 3, Downloaded from http:

ibrary wiley.com/doi/10.1029/2022JB025735, Wiley Online Library on [14/03/2023]. See the Terms

infrasound observations being less feasible and usually not considered in most studies due to their high upper atmosphere absorption (Sutherland & Bass, 2004), our models indicate thermospheric arrivals could explain observations at stations with high crosswinds effects (e.g., IS02 and IS08). Thermospheric paths have been interpreted before for infrasound recorded at IS22, New Caledonia for signals from Lopevi volcano in Vanuatu at a range of ~650 km (Le Pichon, Blanc, Drob, et al., 2005), at IS19 for signals from Nabro volcano at a range of 264 km (Fee et al., 2013), at the LITE array for signals from Tungurahua at a range of 251 km (J. D. Assink et al., 2012), and discussed as a possibility for Calbuco (2015) (Matoza et al., 2018). The long-range propagation for the considered stations (>1,500 km) and possible thermospheric path for 2015 Calbuco and 2011 Cordon Caulle warrants further investigation.

5.2.2. Tropospheric Arrivals

The existence of tropospheric turning heights (\sim <25 km) in the hybrid model case from Calbuco to IS02 (see Figure S10 in Supporting Information S1) suggests considering a third category of arrivals in the search process. However, the modeled backazimuth deviations for tropospheric arrivals are much smaller than the "strato. and thermo." cases (\sim 3° vs. \sim 10°) and we did not find many observations with such deviations values (see Figure S12a in Supporting Information S1). Additionally, tropospheric wind jets tend to have shorter time spans and cover smaller regions (Drob et al., 2003), which are features that will be smoothed out by the empirical climatologies (e.g., Le Pichon, Blanc, & Drob, 2005).

5.2.3. Perturbed Cases

The climatological perturbed models have higher deviation values, generally better matching the observed mean and median observed of the detections. For some of the hybrid results (e.g., IS09 and IS41 for Cordón Caulle), it seems that the Gaussian perturbation introduces an overcorrection that results in an increased overall mislocation (see Figure 7 for Cordón Caulle hybrid "strato. and thermo." cases). When perturbing the empirical climatologies, on the other hand, the source mislocations always reduce for "strato. and thermo." cases, supporting the idea of using a simple Gaussian perturbation to enhance the stratospheric duct effects.

5.3. Source Locations

The completeness of the IMS network is critical for source location purposes (Le Pichon et al., 2009) and this manifests when comparing the Cordón Caulle and Calbuco results. The lack of IS41 detections on April 2015 produces a basal (uncorrected) source mislocation increment of ~120 km for Calbuco when compared to Cordón Caulle, setting a limit on the location accuracy for Calbuco eruption that is clear across our source location results (Figures 7 and 8). Another major factor in the increase or reduction of the source mislocation was the existence of correction values for the most relevant detecting stations. From Figure 8 it is clear that the mislocation increases when applying corrections to a very limited number of stations. For example, the case of perturbed climatologies with only stratospheric arrivals does not find deviations for IS02 and IS08, which are determinant to constrain the source longitude, resulting in a cross-bearing maximum that is actually much farther from the uncorrected location (see Figure 7; also see Figures S13-S18 in Supporting Information S1). The low number of predictions for "only strato." cases shows that the iterative search of arrivals is less effective in converging toward the target station location when using only rays with stratospheric turning heights. We think this could be partially tackled by fine-tuning the iteration launch parameters case by case (e.g., changing the launch azimuths for ISO2 or ISO8), but in this study we kept the same modeling parameters across all cases for consistency (see Text S1 in Supporting Information S1 for more insights of possible improvements in the search algorithm). Nevertheless, the "strato. and thermo." cases are very effective in reducing the source mislocation as they provide robust deviation estimations for nearly all stations. This suggests that when using a cross-bearings approach such as IMS_vASC, the corrections should only be applied if a minimum number of detecting stations is involved. In this study, whenever the stations IS02, IS08, IS09, IS27, and IS41 had associated correction values we obtained a significant source mislocation reduction (Figure 7 and Table 1).

Our results indicate that our automatic climatology-based methodology could provide rapid and robust predictions of the backazimuth deviation for similar source location cases. Applications of this methodology extend to the case of using yearly predictions of backazimuth deviation behavior to discriminate volcanic infrasound from clutter (De Negri et al., 2022). Upon further testing and performance tuning (see Text S1 in Supporting Information S1) we think the method has good potential to be used for studies that involve large temporal and spacial data sets, and also near real-time infrasound location systems.

DE NEGRI AND MATOZA 14 of 18

21699356, 2023, 3, Downloaded from https://agupubs.

elibrary.wiley.com/doi/10.1029/2022JB025735, Wiley Online Library on [14/03/2023]. See

conditions) on Wiley Online Library for rules of use; OA articles are governed by the applicable Creative Commons Licens

5.4. Blind Search

We expect that our approach should generally limit the contribution of clutter (Matoza et al., 2013) and reduce the rate of false associations and detections by limiting the number and spatial distribution of trial source nodes that can be linked for each station (Figure 3). In this sense, a priori trial source nodes could be mapped to specific backazimuth deviation values, or rejected as implausible trial source locations, depending on the time of the year and receiver location, generally improving source location and association capabilities. The present study investigates the degree of mislocation reduction for known sources and the overall feasibility of the method (Figure 3). Further implementation and integration into a blind search algorithm (Matoza et al., 2017) could be explored in future work.

6. Conclusions

We introduce a method for rapid first-order estimates of infrasonic backazimuth deviation to improve source-location procedures for a grid of trial source-receiver pairs based on empirical climatologies (HWM14/ NRLMSIS2.0) and 3-D ray tracing (GeoAc/infraGA). The use of empirical climatologies enables the estimates to be pre-computed a priori, rendering the method suitable for real-time applications or systematic analyses of large infrasound data archives. Our approach prioritizes rapid and efficient computation speed over atmospheric and infrasound propagation realism. We employ a simple Gaussian wind jet profile perturbation parameterization to enhance marginal ducting conditions within reasonable bounds and thus compensate for the missing information on fine-scale atmospheric structure in the empirical climatologies. We evaluate our approach based on infrasound source location case studies for two volcanic eruptions in Chile recorded by the IMS: the 2011 eruption of Puyehue-Cordón Caulle volcanic complex and the 2015 eruption of Calbuco. Overall, we find that our approach using perturbed empirical climatologies provides an improvement in source location compared to having no backazimuth deviation correction. For the two case studies considered, the results using climatological models compare well with results based on realistic hybrid atmospheric specifications (ECMWF ERA 5 reanalysis below ~80 km combined with climatologies for higher altitudes). Thus, a practical workflow for real-time monitoring applications can combine empirical climatologies for rapid first-order source-location estimates, followed later by refined source-location estimates using hybrid atmospheric specifications once available. We emphasize that in this study we used the known volcanic source locations a priori to compute the backazimuth deviations at the stations, with the goal of evaluating the overall approach with climatologies. Extension of the method to a blind search process with a grid of trial source nodes represents future work.

Data Availability Statement

- All IMS data are available for scientific studies through the CTBTO vDEC platform (https://www.ctbto.org/specials/vdec/).
- For the hybrid models we used the CDS API tools freely provided by European Centre for Medium-Range Weather Forecasts (ECMWF) to obtain the necessary ERA5 reanalysis profiles, publicly available for academic research (https://confluence.ecmwf.int/display/CKB/How+to+download+ERA5).
- The climatology (HWM/MSISE) model codes are available from Drob et al. (2015) and Emmert et al. (2020), respectively.
- The code for this project is available for research purposes in the GitHub repository https://github.com/rodrum/arcade along with instructions and examples. The code release used for this work can be accessed through Zenodo in https://doi.org/10.5281/zenodo.7643898 (De Negri, 2023).

References

Arrowsmith, S., Drob, D. P., Hedlin, M. A. H., & Edwards, W. (2007). A joint seismic and acoustic study of the Washington State bolide: Observations and modeling. *Journal of Geophysical Research*, 112(D9), D09304. https://doi.org/10.1029/2006jd008001

Arrowsmith, S., Euler, G., Marcillo, O., Blom, P., Whitaker, R., & Randall, G. (2015). Development of a robust and automated infrasound event catalogue using the International Monitoring System. *Geophysical Journal International*, 200(3), 1411–1422. https://doi.org/10.1093/gji/ggu486

Arrowsmith, S., & Whitaker, R. (2008). Inframonitor: A tool for regional infrasound monitoring. In 2008 Monitoring Research Review: Ground-based nuclear explosion monitoring technologies.

Acknowledgments

This work was funded by NSF Grant EAR-1847736. R.S.D. thanks Dr. Philip Blom for answering questions about the InfraGA/GeoAc software. All International Monitoring System data are available for scientific studies through the CTBTO vDEC platform (https://www.ctbto.org/specials/vdec/). The views expressed herein are those of the authors and do not necessarily reflect the views of the CTBTO Preparatory Commission.

DE NEGRI AND MATOZA 15 of 18

21699356, 2023, 3, Downloaded from https

com/doi/10.1029/2022JB025735, Wiley Online Library on [14/03/2023]. See

- Arrowsmith, S., Whitaker, R., Taylor, S. R., Burlacu, R., Stump, B., Hedlin, M., et al. (2008). Regional monitoring of infrasound events using multiple arrays: Application to Utah and Washington State. *Geophysical Journal International*, 175(1), 291–300. https://doi.org/10.1111/j.1365-246x.2008.03912.x
- Assink, J., Smets, P., Marcillo, O., Weemstra, C., Lalande, J.-M., Waxler, R., et al. (2019). Advances in infrasonic remote sensing methods. In A. Le Pichon, E. Blanc, & A. Hauchecorne (Eds.), Infrasound monitoring for atmospheric studies: Challenges in middle atmosphere dynamics and societal benefits (pp. 605–632). Springer International Publishing, https://doi.org/10.1007/978-3-319-75140-5 18
- Assink, J. D., Pichon, A. L., Blanc, E., Kallel, M., & Khemiri, L. (2014). Evaluation of wind and temperature profiles from ECMWF analysis on two hemispheres using volcanic infrasound. *Journal of Geophysical Research: Atmospheres*, 119(14), 8659–8683. https://doi.org/10.1002/2014jd021632
- Assink, J. D., Waxler, R., & Drob, D. (2012). On the sensitivity of infrasonic traveltimes in the equatorial region to the atmospheric tides. *Journal of Geophysical Research*, 117(D1). https://doi.org/10.1029/2011JD016107
- Blom, P. (2020). The influence of irregular terrain on infrasonic propagation in the troposphere. *Journal of the Acoustical Society of America*, 148, 1984–1997. Acoustical Society of America. https://doi.org/10.1121/10.0002128
- Blom, P., & Waxler, R. (2012). Impulse propagation in the nocturnal boundary layer: Analysis of the geometric component. *Journal of the Acoustical Society of America*, 131(5), 3680–3690. https://doi.org/10.1121/1.3699174
- Brachet, N., Brown, D., Bras, R. L., Cansi, Y., Mialle, P., & Coyne, J. (2010). Monitoring the Earth's atmosphere with the global IMS infrasound network. In *Infrasound monitoring for atmospheric studies* (pp. 77–118). Springer Netherlands. https://doi.org/10.1007/978-1-4020-9508-5_3
- Brown, D. J., Katz, C. N., Bras, R. L., Flanagan, M. P., Wang, J., & Gault, A. K. (2002). Infrasonic signal detection and source location at the prototype International Data Centre. *Pure and Applied Geophysics*, 159(5), 1081–1125. https://doi.org/10.1007/s00024-002-8674-2
- Cansi, Y. (1995). An automatic seismic event processing for detection and location: The P.M.C.C. Method. Geophysical Research Letters, 22(9), 1021–1024. https://doi.org/10.1029/95g100468
- Cansi, Y., & Klinger, Y. (1997). An automated data processing method for mini-arrays. Newsletter of the European-Mediterranean Seismological Center. 11, 2–4.
- Castruccio, A., Clavero, J., Segura, A., Samaniego, P., Roche, O., Pennec, J.-L. L., & Droguett, B. (2016). Eruptive parameters and dynamics of the April 2015 sub-Plinian eruptions of Calbuco volcano (southern Chile). Bulletin of Volcanology, 78(9), 62. https://doi.org/10.1007/s00445-016-1058-8
- Caudron, C., Taisne, B., Garcés, M., Alexis, L., & Mialle, P. (2015). On the use of remote infrasound and seismic stations to constrain the eruptive sequence and intensity for the 2014 Kelud eruption. *Geophysical Research Letters*, 42(16), 6614–6621. https://doi.org/10.1002/2015gl064885
- Ceranna, L., Le Pichon, A., Green, D. N., & Mialle, P. (2009). The Buncefield explosion: A benchmark for infrasound analysis across Central Europe. *Geophysical Journal International*, 177(2), 491–508. https://doi.org/10.1111/j.1365-246x.2008.03998.x
- Christie, D. R., & Campus, P. (2010). The IMS infrasound network: Design and establishment of infrasound stations. In *Infrasound monitoring* for atmospheric studies (pp. 29–75). Springer Netherlands. https://doi.org/10.1007/978-1-4020-9508-5_2
- Collini, E., Osores, M. S., Folch, A., Viramonte, J. G., Villarosa, G., & Salmuni, G. (2013). Volcanic ash forecast during the June 2011 Cordón Caulle eruption. *Natural Hazards*, 66(2), 389–412. https://doi.org/10.1007/s11069-012-0492-y
- Dabrowa, A., Green, D., Rust, A., & Phillips, J. (2011). A global study of volcanic infrasound characteristics and the potential for long-range monitoring. Earth and Planetary Science Letters, 310(3–4), 369–379. https://doi.org/10.1016/j.epsl.2011.08.027
- De Angelis, S., Fee, D., Haney, M., & Schneider, D. (2012). Detecting hidden volcanic explosions from Mt. Cleveland Volcano, Alaska with infrasound and ground-coupled airwaves. *Geophysical Research Letters*, 39(21). https://doi.org/10.1029/2012g1053635
- De Negri, R. (2023). rodrum/arcade: ARCADE first release (Version v1.0) [Computer software]. Zenodo. https://doi.org/10.5281/ZENODO.7643898
- De Negri, R. S., Rose, K. M., Matoza, R. S., Hupe, P., & Ceranna, L. (2022). Long-range Multi-year infrasonic detection of eruptive activity at Mount Michael Volcano, South Sandwich Islands. *Geophysical Research Letters*, 49(7). https://doi.org/10.1029/2021GL096061
- Drob, D. P., Emmert, J. T., Meriwether, J. W., Makela, J. J., Doornbos, E., Conde, M., et al. (2015). An update to the Horizontal Wind Model (HWM): The quiet time thermosphere. *Earth and Space Science*, 2(7), 301–319. https://doi.org/10.1002/2014ea000089
- Drob, D. P., Garcés, M., Hedlin, M., & Brachet, N. (2010). The Temporal Morphology of infrasound propagation. *Pure and Applied Geophysics*, 167(4–5), 437–453. https://doi.org/10.1007/s00024-010-0080-6
- Drob, D. P., Meier, R. R., Picone, J. M., & Garcés, M. M. (2010). Inversion of infrasound signals for passive atmospheric remote sensing. In *Infrasound monitoring for atmospheric studies* (pp. 701–731). Springer Netherlands. https://doi.org/10.1007/978-1-4020-9508-5_24
- Drob, D. P., Picone, J. M., & Garcés, M. (2003). Global morphology of infrasound propagation. *Journal of Geophysical Research*, 108(D21). https://doi.org/10.1029/2002id003307
- Elissondo, M., Baumann, V., Bonadonna, C., Pistolesi, M., Cioni, R., Bertagnini, A., et al. (2016). Chronology and impact of the 2011 Cordón Caulle eruption, Chile. *Natural Hazards and Earth System Sciences*, 16(3), 675–704. https://doi.org/10.5194/nhess-16-675-2016
- Emmert, J. T., Drob, D. P., Picone, J. M., Siskind, D. E., Jones, M., Mlynczak, M. G., et al. (2020). NRLMSIS 2.0: A whole-atmosphere empirical model of temperature and neutral Species densities. Earth and Space Science, 8(3). https://doi.org/10.1029/2020ea001321
- Evers, L., & Haak, H. (2005). The detectability of infrasound in The Netherlands from the Italian volcano Mt. Etna. *Journal of Atmospheric and Solar-Terrestrial Physics*, 67(3), 259–268. https://doi.org/10.1016/j.jastp.2004.09.002
- Evers, L., & Haak, H. (2007). Infrasonic forerunners: Exceptionally fast acoustic phases. Geophysical Research Letters, 34(10), L10806. https://doi.org/10.1029/2007g1029353
- Fee, D., Bishop, J., Waxler, R., & Matoza, R. (2020). Infrasound propagation working group (IPWG) report (Vol. 9). Wilson Alaska Technical Center, Geophysical Institute, University of Alaska Fairbanks. Retrieved from https://watc.alaska.edu/sites/default/files/2021-06/IPWG%20 Report_final.pdf
- Fee, D., Garces, M., & Steffke, A. (2010). Infrasound from Tungurahua Volcano 2006–2008: Strombolian to Plinian eruptive activity. *Journal of Volcanology and Geothermal Research*, 193(1–2), 67–81. https://doi.org/10.1016/j.jvolgeores.2010.03.006
- Fee, D., Matoza, R. S., Gee, K. L., Neilsen, T. B., & Ogden, D. E. (2013). Infrasonic crackle and supersonic jet noise from the eruption of Nabro Volcano, Eritrea. *Geophysical Research Letters*, 40(16), 4199–4203. https://doi.org/10.1002/grl.50827
- Garcés, M. (2004). On using ocean swells for continuous infrasonic measurements of winds and temperature in the lower middle, and upper atmosphere. Geophysical Research Letters, 31(19), L19304. https://doi.org/10.1029/2004gl020696
- Garcés, M., Fee, D., Steffke, A., McCormack, D., Servranckx, R., Bass, H., et al. (2008). Capturing the acoustic fingerprint of stratospheric ash injection. Eos Transactions American Geophysical Union, 89(40), 377–378. https://doi.org/10.1029/2008eo400001
- Gibson, R., Drob, D., & Broutman, D. (2009). Advancement of techniques for modeling the effects of fine-scale atmospheric inhomogeneities on infrasound propagation. Proceedings of the 2009 Monitoring Research Review: Ground-Based Nuclear Explosion Monitoring Technologies, LA-UR-08, 5276, pp. 714-728.

DE NEGRI AND MATOZA 16 of 18

- Global Volcanism Program. (2013). Global Volcanism Program—Volcanoes of the World v. 4.5.3. In E. Venzke (Ed.), Smithsonian Institution. https://doi.org/10.5479/si.GVP.VOTW4-2013. (Accessed on June 2016).
- Green, D. N., & Bowers, D. (2010). Estimating the detection capability of the International Monitoring System infrasound network. *Journal of Geophysical Research*, 115(D18), D18116. https://doi.org/10.1029/2010jd014017
- Green, D. N., Evers, L., Fee, D., Matoza, R., Snellen, M., Smets, P., & Simons, D. (2013). Hydroacoustic infrasonic and seismic monitoring of the submarine eruptive activity and sub-aerial plume generation at South Sarigan, May 2010. *Journal of Volcanology and Geothermal Research*, 257, 31–43. https://doi.org/10.1016/j.jvolgeores.2013.03.006
- Green, D. N., Vergoz, J., Gibson, R., Le Pichon, A., & Ceranna, L. (2011). Infrasound radiated by the Gerdec and Chelopechene explosions: Propagation along unexpected paths. *Geophysical Journal International*, 185(2), 890–910. https://doi.org/10.1111/j.1365-246x.2011.04975.x Jones, R. M. (1986). *HARPA manual*. US Department of Commerce.
- Kamo, K., Ishihara, K., & Tahira, M. (1994). Infrasonic and seismic detection of explosive eruption at Sakurajima Volcano, Japan, and the PEGASAS-VE early-warning system.
- Kulichkov, S. N., Chunchuzov, I. P., & Popov, O. I. (2010). Simulating the influence of an atmospheric fine inhomogeneous structure on long-range propagation of pulsed acoustic signals. *Izvestiya - Atmospheric and Oceanic Physics*, 46(1), 60–68. https://doi.org/10.1134/ s0001433810010093
- Lalande, J.-M., & Waxler, R. (2016). The interaction between infrasonic waves and gravity wave perturbations: Application to observations using UTTR Rocket Motor Fuel Elimination Events. *Journal of Geophysical Research: Atmospheres*, 121(10), 5585–5600. https://doi.org/10.1002/2015JD024527
- Le Pichon, A., Assink, J. D., Heinrich, P., Blanc, E., Charlton-Perez, A., Lee, C. F., et al. (2015). Comparison of co-located independent ground-based middle atmospheric wind and temperature measurements with numerical weather prediction models. *Journal of Geophysical Research: Atmospheres*, 120(16), 8318–8331. https://doi.org/10.1002/2015jd023273
- Le Pichon, A., Blanc, E., & Drob, D. (2005). Probing high-altitude winds using infrasound. *Journal of Geophysical Research*, 110(D20), D20104. https://doi.org/10.1029/2005jd006020
- Le Pichon, A., Blanc, E., Drob, D., Lambotte, S., Dessa, J., Lardy, M., & Vergniolle, S. (2005). Infrasound monitoring of volcanoes to probe high-altitude winds. *Journal of Geophysical Research*, *110*(D13), D13106. https://doi.org/10.1029/2004jd005587
- Le Pichon, A., Ceranna, L., Garcés, M., Drob, D., & Millet, C. (2006). On using infrasound from interacting ocean swells for global continuous measurements of winds and temperature in the stratosphere. *Journal of Geophysical Research*, 111(D11), D11106. https://doi.org/10.1029/2005jd006690
- Le Pichon, A., Vergoz, J., Blanc, E., Guilbert, J., Ceranna, L., Evers, L., & Brachet, N. (2009). Assessing the performance of the International Monitoring System's infrasound network: Geographical coverage and temporal variabilities. *Journal of Geophysical Research*, 114(D8). D08112. https://doi.org/10.1029/2008id010907
- Le Pichon, A., Vergoz, J., Herry, P., & Ceranna, L. (2008). Analyzing the detection capability of infrasound arrays in Central Europe. *Journal of Geophysical Research*, 113(D12), D12115. https://doi.org/10.1029/2007jd009509
- Marchetti, E., Ripepe, M., Campus, P., Pichon, A. L., Brachet, N., Blanc, E., et al. (2019). Infrasound Monitoring of Volcanic eruptions and contribution of ARISE to the Volcanic Ash Advisory Centers. In *Infrasound monitoring for atmospheric studies* (pp. 1141–1162). Springer International Publishing. https://doi.org/10.1007/978-3-319-75140-5_36
- Marcillo, O., Arrowsmith, S., Whitaker, R., Anderson, D., Nippress, A., Green, D. N., & Drob, D. (2014). Using physics-based priors in a Bayesian algorithm to enhance infrasound source location. *Geophysical Journal International*, 196(1), 375–385. https://doi.org/10.1093/gjj/ggt353
- Matoza, R., Fee, D., Green, D., & Mialle, P. (2019). Volcano infrasound and the International Monitoring system. In Infrasound monitoring for atmospheric studies (pp. 1023–1077). Springer International Publishing. https://doi.org/10.1007/978-3-319-75140-5_33
- Matoza, R., Fee, D., Green, D. N., Le Pichon, A., Vergoz, J., Haney, M. M., et al. (2018). Local, regional, and remote seismo-acoustic observations of the April 2015 VEI 4 eruption of Calbuco Volcano, Chile. *Journal of Geophysical Research: Solid Earth*, 123(5), 3814–3827. https://doi.org/10.1002/2017jb015182
- Matoza, R., Green, D. N., Pichon, A. L., Shearer, P. M., Fee, D., Mialle, P., & Ceranna, L. (2017). Automated detection and cataloging of global explosive volcanism using the International Monitoring System infrasound network. *Journal of Geophysical Research: Solid Earth*, 122(4), 2946–2971. https://doi.org/10.1002/2016jb013356
- Matoza, R., Hedlin, M. A., & Garcés, M. A. (2007). An infrasound array study of Mount St. Helens. *Journal of Volcanology and Geothermal Research*, 160(3–4), 249–262. https://doi.org/10.1016/j.jvolgeores.2006.10.006
- Matoza, R., Landès, M., Le Pichon, A., Ceranna, L., & Brown, D. (2013). Coherent ambient infrasound recorded by the International Monitoring System. *Geophysical Research Letters*, 40(2), 429–433. https://doi.org/10.1029/2012gl054329
- Matoza, R., Le Pichon, A., Vergoz, J., Herry, P., Lalande, J.-M., il Lee, H., et al. (2011). Infrasonic observations of the June 2009 Sarychev Peak eruption Kuril Islands: Implications for infrasonic monitoring of remote explosive volcanism. *Journal of Volcanology and Geothermal Research*, 200(1–2), 35–48. https://doi.org/10.1016/j.jvolgeores.2010.11.022
- Matoza, R., Vergoz, J., Le Pichon, A., Ceranna, L., Green, D. N., Evers, L., et al. (2011). Long-range acoustic observations of the Eyjafjallajökull eruption, Iceland, April-May 2010. *Geophysical Research Letters*, 38(6). https://doi.org/10.1029/2011g1047019
- Mialle, P., Brachet, P., Gaillard, A., Le Pichon, A., Blanc, D., Tailpied, E., & Friha, N. (2015). Towards a volcanic notification system with infrasound data: Use of infrasound data in support of the VAACs in the framework of ARISE project. In World Meteorological Organization 7th International Workshop on Volcanic Ash (IWVA/7), Anchorage, Alaska.
- Mialle, P., Brown, D., Arora, N., & colleages from IDC (2019). Advances in Operational processing at the International Data Centre. In Infrasound monitoring for atmospheric studies (pp. 209–248). Springer International Publishing. https://doi.org/10.1007/978-3-319-75140-5_6
- Modrak, R. T., Arrowsmith, S., & Anderson, D. N. (2010). A Bayesian framework for infrasound location. *Geophysical Journal International*, 181(1), 399–405. https://doi.org/10.1111/j.1365-246x.2010.04499.x
- Morton, E. A., & Arrowsmith, S. (2014). The development of global probabilistic propagation look-up tables for infrasound celerity and back-azimuth deviation. Seismological Research Letters, 85(6), 1223–1233. https://doi.org/10.1785/0220140124
- Newhall, C. G., & Self, S. (1982). The volcanic explosivity index (VEI) an estimate of explosive magnitude for historical volcanism. *Journal of Geophysical Research*, 87(C2), 1231. https://doi.org/10.1029/jc087ic02p01231
- Geophysical Research, 8/(C2), 1231. https://doi.org/10.1029/jc08/ic02p01231
 Nippress, A., Green, D. N., Marcillo, O. E., & Arrowsmith, S. (2014). Generating regional infrasound celerity-range models using ground-truth
- information and the implications for event location. Geophysical Journal International, 197(2), 1154–1165. https://doi.org/10.1093/gji/ggu049
 Norris, D., Gibson, R., & Bongiovanni, K. (2010). Numerical Methods to Model infrasonic propagation through realistic specifications of the atmos-
- phere. In *Infrasound monitoring for atmospheric studies* (pp. 541–573). Springer Netherlands. https://doi.org/10.1007/978-1-4020-9508-5_17 Park, J., Arrowsmith, S., Hayward, C., Stump, B. W., & Blom, P. (2014). Automatic infrasound detection and location of sources in the Western United States. *Journal of Geophysical Research: Atmospheres*, 119(13), 7773–7798. https://doi.org/10.1002/2013jd021084

DE NEGRI AND MATOZA 17 of 18

- Perttu, A., Taisne, B., De Angelis, S., Assink, J. D., Tailpied, D., & Williams, R. A. (2020). Estimates of plume height from infrasound for regional volcano monitoring. *Journal of Volcanology and Geothermal Research*, 402, 106997. https://doi.org/10.1016/j.jvolgeores.2020.106997
- Ripepe, M., Marchetti, E., Donne, D. D., Genco, R., Innocenti, L., Lacanna, G., & Valade, S. (2018). Infrasonic early warning system for explosive eruptions. *Journal of Geophysical Research: Solid Earth*, 123(11), 9570–9585. https://doi.org/10.1029/2018jb015561
- Sanderson, R. W., Matoza, R., Fee, D., Haney, M. M., & Lyons, J. J. (2020). Remote detection and location of explosive Volcanism in Alaska with the EarthScope transportable array. *Journal of Geophysical Research: Solid Earth*, 125(4). https://doi.org/10.1029/2019jb018347
- Schwaiger, H. F., Iezzi, A. M., & Fee, D. (2019). AVO-G2S: A modified open-source ground-to-space atmospheric specification for infrasound modeling. Computers & Geosciences, 125, 90–97. https://doi.org/10.1016/j.cageo.2018.12.013
- Smets, P. S. M., Assink, J. D., Pichon, A. L., & Evers, L. (2016). ECMWF SSW forecast evaluation using infrasound. *Journal of Geophysical Research: Atmospheres*, 121(9), 4637–4650. https://doi.org/10.1002/2015jd024251
- Smets, P. S. M., Evers, L., Näsholm, S. P., & Gibbons, S. J. (2015). Probabilistic infrasound propagation using realistic atmospheric perturbations. Geophysical Research Letters, 42(15), 6510–6517. https://doi.org/10.1002/2015gl064992
- Sutherland, L. C., & Bass, H. E. (2004). Atmospheric absorption in the atmosphere up to 160 km. *Journal of the Acoustical Society of America*, 115(3), 1012–1032. https://doi.org/10.1121/1.1631937
- Taisne, B., Perttu, A., Tailpied, D., Caudron, C., & Simonini, L. (2019). Atmospheric controls on ground- and space-based remote detection of volcanic ash injection into the atmosphere and link to early warning systems for aviation hazard mitigation. In *Infrasound monitoring for atmospheric studies* (pp. 1079–1105). Springer International Publishing. https://doi.org/10.1007/978-3-319-75140-5_34
- Van Eaton, A. R., Amigo, Á., Bertin, D., Mastin, L. G., Giacosa, R. E., González, J., et al. (2016). Volcanic lightning and plume behavior reveal evolving hazards during the April 2015 eruption of Calbuco volcano, Chile. Geophysical Research Letters, 43(7), 3563–3571. https://doi. org/10.1002/2016gl068076
- Walker, K. T., & Hedlin, M. A. (2010). A review of wind-noise reduction methodologies. In *Infrasound monitoring for atmospheric studies* (pp. 141–182). Springer Netherlands. https://doi.org/10.1007/978-1-4020-9508-5_5
- Waxler, R., Assink, J., & Velea, D. (2017). Modal expansions for infrasound propagation and their implications for ground-to-ground propagation. *Acoustical Society of America*, 141(2), 1290–1307. https://doi.org/10.1121/1.4976067

DE NEGRI AND MATOZA 18 of 18